Journal of the European Ceramic Society 20 (2000) 983–990

# Dense ceramics of $NaNbO_3$ produced from powders prepared by a new chemical route

S. Lanfredi [a,1], L. Dessemond [a,*], A.C. Martins Rodrigues [b]

[a] *Laboratoire d' Electrochimie et de Physicochimie des Matériaux et des Interfaces, UMR 5631 INPG-CNRS, Institut National Polytechnique de Grenoble, ENSEEG, 1130 Rue de la Piscine, BP 75, Domaine Universitaire, 38402 Saint Martin D'Heres Cedex, France*

[b] *Departamento de Engenhariza de Materiais, Universidade Federal De São Carlos, UFSCar, C.P. 676, 13565-905 São Carlos, S.P., Brazil*

Received 10 January 1998; received in revised form 20 July 1999; accepted 8 August 1999

**Abstract**

A sodium niobate precursor was prepared by evaporating a solution of an oxalato-niobium complex, sodium nitrate, oxalic acid and ammonium hydroxide. The thermal evolution of the precursor powder, to the point of formation of the $NaNbO_3$ phase, was followed by thermal analysis and powder X-ray diffraction. Calcination of the precursor above 500°C for 5 h in air yielded a pure single phase $NaNbO_3$. The non-isothermal densification behaviour was followed by dilatometric measurements. Highly sinterable powders were prepared by this new chemical route. Densities higher than 95% of the theoretical one were reached after sintering at 1250°C for 2 h in air. 

*Keywords:* Calcination; $NaNbO_3$; Niobates; Powders-chemical preparation; Sintering

## 1. Introduction

Sodium niobate is a dielectric material of the perovskite group. This material undergoes a series of structural transitions between 200 and 640°C.[1] At room temperature, $NaNbO_3$ presents an orthorhombic symmetry,[2] while above 640°C, it has the ideal perovskite structure with a cubic symmetry.[3] At room temperature, $NaNbO_3$ is antiferroelectric and ferroelectricity has been observed below 0°C.[4] The addition of $LiNbO_3$ to $NaNbO_3$, even in small amounts, produces a new ferroelectric phase which makes polycrystalline lithium sodium niobate ceramics suitable for high frequency device applications.[5–8] The variations of the Curie temperature of $NaNbO_3$ based solid solutions caused by different concentrations of $LiNbO_3$[9] suggest that piezoelectric, pyroelectric, electrooptic and ferroelastic applications may be expected. Despite these promising electrical properties, few studies have so far been carried out on the synthesis and sintering of polycrystalline sodium niobate. Such an investigation would be relevant since the electrical and optical properties of dielectric ceramics strongly depend on their microstructure,[10,11] which is mainly influenced by the powder synthesising method and sintering process.

Alkali metal niobates powders are usually synthesized via a solid state reaction route using sodium and/or lithium carbonates and niobium pentoxide.[12–15] One of the characteristics of this classical method is that it is rather difficult to achieve an homogeneous mixture of the components. Moreover, high sintering temperatures are required because of the low surface area of raw powders. Indeed, this method does not always allow for the production of dense, homogeneous single phase ceramics. High sintering temperatures can also enhance the volatilization of the alkali metal, which leads to stoichiometric variations in the sintered material.

Increased sinterability of mixed powders and higher densification rate of green compacts were attained through pressure sintering and/or by adding selected sintering additives.[16–19] Fired densities ranging from 94 to 98% of the theoretical ones were thus reached. The firing temperature was decreased by one hundred degrees using pressure sintering. However, a calcination step at a temperature of around 900°C and a subsequent annealing in an oxygen flow were sometimes required.[6,7]

A method to prepare transparent ferroelectric glass-ceramics based on metal alkali niobates by a direct crystallization of a batch of oxides was recently proposed.[20] The reported results suggest that as-prepared

* Corresponding author. Tel.: +33-76-82-6500; fax: +33-7682-67770.
*E-mail address:* lepmi@ccomm.grenet.fr (L. Dessemond).

[1] On leave from Departamento de Quimica, Universidade Federal De Sao Carlos, UFSCar, C.P. 13565-905 Sao Carlos, S.P., Brazil.

0955-2219/00/$ - see front matter 
PII: S0955-2219(99)00223-X

materials are suitable for electrooptical applications, but the temperatures required exceed 1350°C.

In recent years, a wide variety of chemical routes for powder synthesis have been developed and optimized for preparing niobate-based electroceramics. The most popular routes are coprecipitation and sol–gel processes.[21] Other alternative methods to prepare ceramic powders have been described in the literature, such as hydrothermal synthesis[22] and a polymeric precursor process derived from the Pechini method.[22–25]

This work reports on a new chemical route to prepare highly sinterable sodium niobate powders to produce dense ceramic bodies. This method uses a precursor powder obtained by evaporation of a starting solution containing an oxalato-niobium complex, sodium nitrate, oxalic acid and ammonium hydroxide. After evaporation, calcination of the precursor powder yielded the single phase $NaNbO_3$. Calcination temperatures were as low as 900°C. The thermal decomposition of the precursor was followed by thermogravimetric analysis (TGA), differential analysis (DTA) and X-ray diffraction (XRD). The sintering behaviour of compacted bodies was studied by dilatometry and the microstructure of sintered samples was examined by scanning electron microscopy (SEM). This evaporative method, employing the same niobium soluble complex has been already proposed for lithium niobate.[26]

## 2. Experimental procedure

### 2.1. Powder preparation

The sodium niobate precursor powder was prepared according to the following procedure. A saturated solution of oxalic acid was initially added to 1 M solution of sodium nitrate (Merck, Germany) in deionized water until pH = 1 (the pH values of the solutions were monitored by pH-metry). The pH value was raised to 3 by addition of a 1:1 ammonium hydroxide solution, which resulted in the formation of sodium oxalate. A solution of 0.7 M ammonium dihydrogen tri(oxalato) oxoniobate (V) trihydrate, $NH_4H_2$ $[NbO(C_2O_4)_3].3H_2O$ (Companhia Brasileira de Metalurgia e Mineração, Brazil) was then added. The final pH value was 2. Low pH values are needed to prevent the precipitation of sodium oxalate and niobium pentoxide.[27,28] Moreover, no precipitation of ammonium oxalate was observed. The final solution was then refluxed at 80°C for 3 h. After refluxing, the solution was maintained at 70°C until complete evaporation of the solvent and formation of the precursor powder was achieved. This powder was then ground in an agate mortar. After the grinding step, the powder was stored in a dessicator owing to the hygroscopic nature of sodium. The as-prepared powder was deposited on an alumina substrate and then calcined between 250 and 900°C for 5 h in air.

### 2.2. Powder characterization

The thermal decomposition of the precursor powder was followed by thermogravimetry and differential thermal analysis using a differential thermal analyser (STA 409, Netzch) under dry air between room temperature and 900°C. The heating rate was fixed at 10°C/min.

The as-prepared and calcined powders were characterized by X-ray diffraction using $CuK_\alpha$ radiation (D5000, Kristalloflex-Siemens). The crystallite mean size, $D$, was calculated from the Scherrer equation:[29]

$$D = \frac{0.9\lambda}{\beta \cos\theta} \tag{1}$$

where $\lambda$ is the wavelength of the $CuK_\alpha$ radiation, $\theta$ the diffraction angle and $\beta$ the width of the diffraction peak at half-maximum intensity at the selected angle given by the following equation:

$$\beta = \left(B_m^2 - b^2\right)^{1/2} \tag{2}$$

where $B_m$ is the measured breadth at half-maximum of the selected diffraction line of the sample and $b$ is that of an internal standard mica crystal in the plane (001).

### 2.3. Compaction and sintering behaviour

Sodium niobate powders used for compaction and densification studies were calcined at 900°C for 5 h in air. The compaction behaviour was studied by varying uniaxial pressure from 40 to 450 MPa. The non-isothermal sintering behaviour was monitored using dilatometry (DI24, Adamel) at constant heating and cooling rates (2°C/min), in air, from room temperature to 1250°C with an isothermal dwell at 1250°C for 1 h. Isothermal densification behaviour was also examined in air by varying temperatures between 1100 and 1250°C, for soaking times up to 2 h. The heating rate to the dwells was 10°C/min and the cooling rate was fixed by the thermal inertia of the furnace.

Green compact and sintered body densities were determined from the measurements of the sample size parameters and weights. Sintered compact microstructures were examined by scanning electron microscopy (JSM 6400, Jeol) on polished surfaces of the samples. The crystalline structure of sintered sodium niobate was characterized by X-ray diffraction.

## 3. Results and discussion

### 3.1. Thermal analysis

Fig. 1 illustrates the thermal decomposition of the precursor. The overall weight loss was 80.8% from

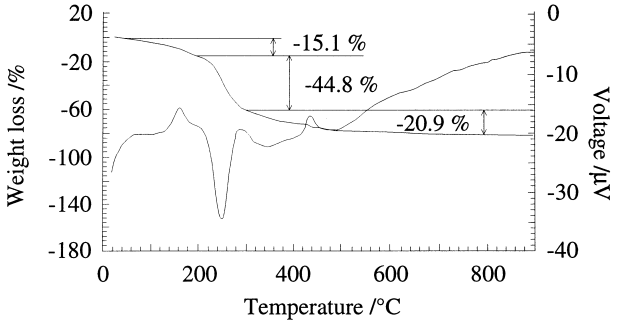


Fig. 1. TGA/DTA curves (10°C/min) of $NaNbO_3$ precursor powder.

room temperature to 900°C. Between 25 and 200°C, the initial weight loss was 15.1%. Generally, the departure of water molecules during thermal decomposition of an oxalato-niobium complex is depicted by one or more endothermic peaks in this temperature range, the magnitude of which depends on the synthesis process.[30,31] The corresponding endothermic effect is likely to be lower in the case of the precursor stored in a dessicator before measurements. Moreover, this peak can be viewed as overlapping with the exothermic effect observed at 158°C (Fig. 1). This latter thermal effect is likely related to the combustion of organic groups. A partial thermal decomposition of an oxalate group of the precursor might be considered although this reaction was generally observed at higher temperatures.[30–32] On the TGA curve (Fig. 1), the highest weight loss (44.8%) occurred between 200 and 300°C, indicating a large elimination of organic material. The DTA analysis shows a corresponding intense endothermic peak at 247°C. This endotherm may be related to the release of water molecules, ammonium ions and CO and $CO_2$ molecules developed by the combustion of organic ligands, which led to the formation of an intermediate oxalato-niobate complex.[30]

Heating above 300°C caused a weight loss of 20.9%. In this temperature range, the DTA curve evidences a weak endotherm at 340°C and a stronger exothermic effect at 431°C. The former may be attributed to the thermal decompostion of the intermediate complex into partly amorphous sodium niobate, as confirmed by XRD analysis (Fig. 2), and to the departure of carbon monoxide and carbon dioxide. The thermal decompostion of simple or complex oxalates occurred with formation of CO and $CO_2$, which may remain adsorbed on the surface of solid products.[32] This decomposition was accompanied by adsorption of carbon monoxide on the vitreous $NaNbO_3$. Further heating led to the desorption of CO above 400°C. Exothermic crystallization of the sodium niobate phase was observed at 431°C (Fig. 1).

No weight loss and no thermal effect was observed above 500°C, indicating that no decomposition occurs above that temperature. Increased temperatures enhances the crystallinity of the calcined powder as confirmed by XRD analysis.

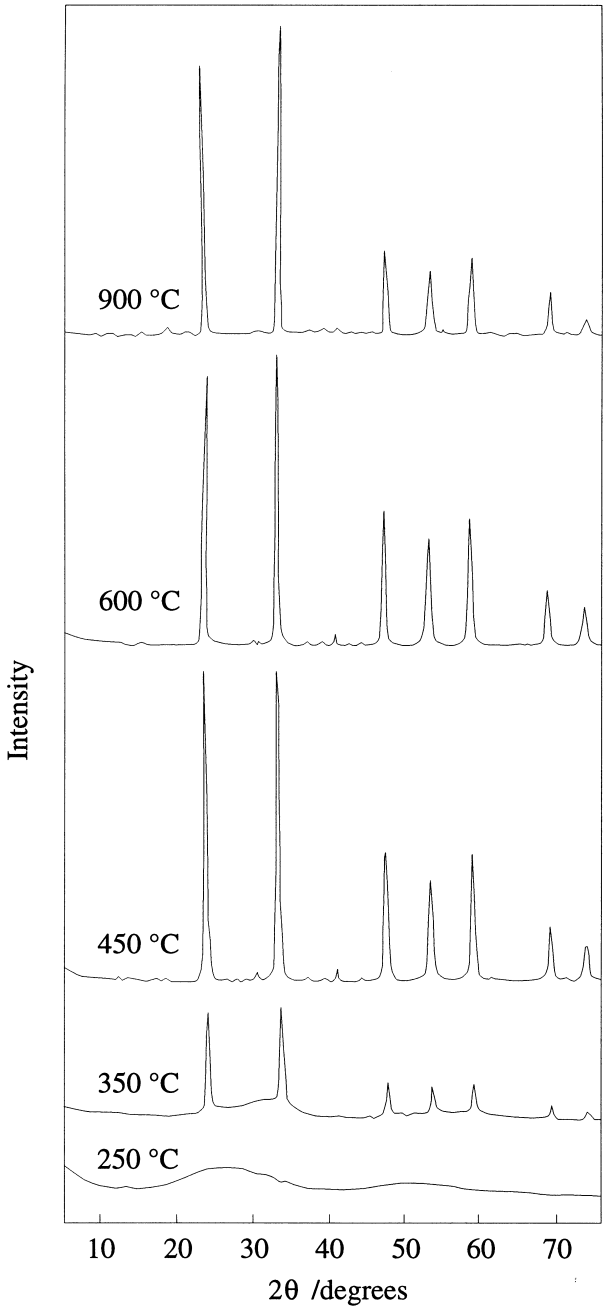


Fig. 2. XRD patterns of $NaNbO_3$ precursor powder heat treated at various temperatures for 5 h.

### 3.2. X-ray diffraction analysis

The XRD diffraction patterns of the $NaNbO_3$ precursor powder heated at temperatures up to 900°C for 5 h are given in Fig. 2. Uncalcined powder (not shown in Fig. 2) and powder calcined at 250°C were both amorphous. The diffraction peaks of powder calcined at 350°C suggest the onset of crystallization of the sodium niobate phase, which was confirmed by further heatings. The $NaNbO_3$ nucleation temperature is close to that determined for powder synthesized via a polymeric

precursor.[23] This temperature is much lower than by using a mixed oxide powder process[13,14] which lies in the 700°C range. During the course of calcination, an increase in the temperature resulted in a simultaneous increase in diffraction peak intensities and a decrease in their breadths. The higher the calcination temperature, the higher the crystallinity of the powder.

From Eq. (2), the mean crystallite size $D$ of calcined powders was determined as a function of calcination temperature. The corresponding values are reported in Table 1. Even after calcination at 900°C, $D$ is lower than 100 nm, which is the usual lowest limit of most commercial powders.[33] The crystallite sizes obtained were almost identical to those measured by Nobre et al.,[23] at least up to 800°C. The low $D$ values suggest that the surface area of the as-calcined powders were sufficiently high to promote a high sinterability. The sintering behaviour of the calcined powders support this assumption.

The XRD patterns of calcined powders are characteristic of the orthorhombic phase of $NaNbO_3$.[34] The XRD analysis showed that no additional crystalline phase formed during calcination up to 900°C. The lattice parameters (of the powders calcined at 900°C) determined at room temperature via a least-square method were: $a = 5.598$ Å, $b = 15.523$ Å and $c = 5.505$ Å. These values are in agreement with previously published data on orthorhombic $NaNbO_3$.[9,23]

The as-prepared powder was white, as were the calcined powders (regardless the firing temperature). This indicates that the powders investigated were devoid of carbon chars.

### 3.3. Chemical analysis

A chemical analysis of the sodium niobate precursor heated at 900°C confirmed that the $NaNbO_3$ phase was stoichiometric, displaying 57.2 wt% Nb and 14.2 wt% Na, which corresponds to a $\frac{Nb}{Na}$ mole ratio of 0.98. These values are in agreement with the expected ones: 55.7 wt% Nb and 14.0 wt% Na. After sintering at 1250°C for 2 h in air, the same $\frac{Nb}{Na}$ mol ratio was found indicating that the stoichiometry of $NaNbO_3$ did not vary by firing at temperatures above 1000°C.

### 3.4. Compaction behaviour

The compaction behaviour of the $NaNbO_3$ powder was studied using a compaction response diagram[35] which relates the relative density (expressed in % of the theoretical one) of the compacts to the logarithm of the uniaxial applied pressure. A typical response diagram shows several straight line segments. The intersection of two linear portions, or the changes in slope of these straight line segments, are the most important features.[36–39] Fig. 3 shows the relationship between the green density and the pressure logarithm for a sodium niobate powder. Four linear regions and three intersections in the relations can be seen in the pressure range investigated. Between 40 and 175 MPa, the relative density is an increasing function of the applied pressure. Assuming a linear variation, a slope of 9.2%/MPa was determined. In the case of $ZrO_2$–$Y_2O_3$ powders synthesized by wet chemical processes, the slope of the linear part corresponding to the deformation and/or the breaking of agglomerates was reported to vary between 8 and 23%/MPa.[33–37,39] Below the low pressure breakpoint, which can be viewed as an estimation of the agglomerate strength, the slope was typically lower than 5%/MPa. Therefore, the observed breakpoint around 175 MPa (Fig. 3) does not correspond to the yielding point of agglomerates in calcined powders. Moreover, the low pressure linear variation corresponds to the rearrangement occuring during and after crushing or deformation of soft agglomerates. All these results suggest that the strength of soft agglomerates is lower than or close to 40 MPa.

The line slope was smaller between 175 and 250 MPa (Fig. 3). In this pressure range, the compaction behaviour is similar to that of agglomerated raw powder. This can be explained in terms of rearrangement of hard agglomerates.[33] Fig. 3 shows a further increase of the line slope above 250 MPa. Between 250 and 320 MPa, the compact density increases from 59 to 65% of the theoretical one. Such high green densities values (as well as those reached by the compaction sequence

Table 1
Mean crystallite size, $D$, of $NaNbO_3$ powder calcined at different temperatures for 5 h

| Calcination temperature°C | 350 | 450 | 600 | 800 | 900 |
|---|---|---|---|---|---|
| $D$/nm | 30 | 32 | 41 | 60 | 85 |

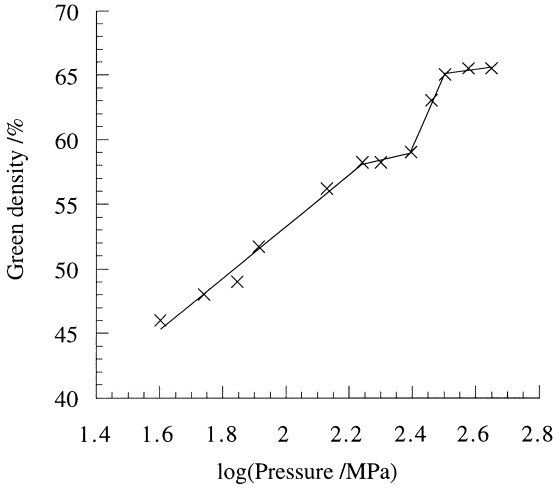


Fig. 3. Compaction response diagram of $NaNbO_3$ powder calcined at 900°C for 5 h.

described below) indicate the excellent packing ability of the calcined powders. According to Matsumoto,[36] such a large change in green density with pressure is indicative of gross residual porosity because of the higher strength of hard agglomerates. No increase in the green density was achieved by exceeding 350 MPa.

### 3.5. Densification behaviour

The sodium niobate powders were pressed uniaxially at 100 MPa and then isostatically at 210 MPa. The green density was 59% of the theoretical one. Increasing the isostatic pressure did not yield to significantly higher green densities. The non-isothermal densification behaviour of $NaNbO_3$ powder is illustrated in [Fig. 4(a)] by the linear shrinkage curve and its derivative versus temperature. As can be seen, a small expansion occurred up to 900°C owing to the dilatation of the material. A significant shrinkage was achieved in the short temperature interval of 250°C between 1000 and 1250°C. At 1250°C, the total linear shrinkage is 17.7% for isopressed powders. Narrow temperature ranges of high densification have also been observed during sintering of metal alkali niobates synthesized by other wet chemical processes.[23,40] The sintering process is not ended at 1250°C, as revealed by the shrinkage that occured during the isothermal dwell [Fig. 4(b)]. After 1 h at 1250°C, the total linear shrinkage is 18.7%. The relative density was then as high as 96% of the theoretical density. It is worth noting, that sodium niobate nearly fully densified only by using pressureless sintering. No dedensification step was observed on the dilatometric curves during sintering. In the case of a mixed powders process, hot-pressure or activated sintering are required to achieve such high density values.[6,16–19,41]

The shrinkage rate increased gradually at temperatures higher than 1000°C, reaching a maximum around 1070°C [Fig. 4(a)]. Subsequently, the sintering process slowed down until reaching the vicinity of 1130°C and a second maximum appears at 1200°C, followed by another decrease at higher temperatures. The maximum densification rate was determined at a temperature as low as 1200°C, demonstrated the high sinterability of powders calcined at 900°C. Such successive peaks on the shrinkage plot have already been observed for $NaNbO_3$ powders prepared from polymeric precursors.[23]

The occurrence of two maxima on the linear shrinkage rate curve has been reported in the literature and can be considered as typical features of a duplex shrinkage. These maxima have been attributed to a regular shrinkage of the monolithic matrix and to either the formation of a new phase,[42,43] the phase transformation of a component,[44,45] or to a heterogeneous densification of the matrix.[46] Powder compact pore size distributions and powder morphology were not determined in this study. However, the observed sintering behaviour may be related to the agglomeration state of calcined powders,[47] as suggested by the compaction behaviour (Fig. 3). The strong influence of green compact density and pore size distribution on sintering kinetics has already been mentioned in the literature.[48–52] The derivative curve of shrinkage versus temperature exhibits only one maximum for deagglomerated $BaTiO_3$ powders. When the powders are non-deagglomerated, the sintering curve shows a second maximum connected to the agglomeration state of powders.[37] The presence of only one maximum in the densification rate curve of nanocrystalline Y-TZP powders confirmed the single mode and narrow pore size distribution in the compacted samples.[39] The sintering behaviour of green samples would, thus, be affected by the agglomerates in powders. Another conceivable sintering mechanism can be considered. A two-step shrinking can also be viewed as characteristic of a liquid-phase-assisted sintering.[53] The first densification peak observed on the shrinkage rate curve of commercial BaTiO3 powders[54] was ascribed to normal grain growth. An abnormal grain growth (resulting from the presence of a liquid phase at grain

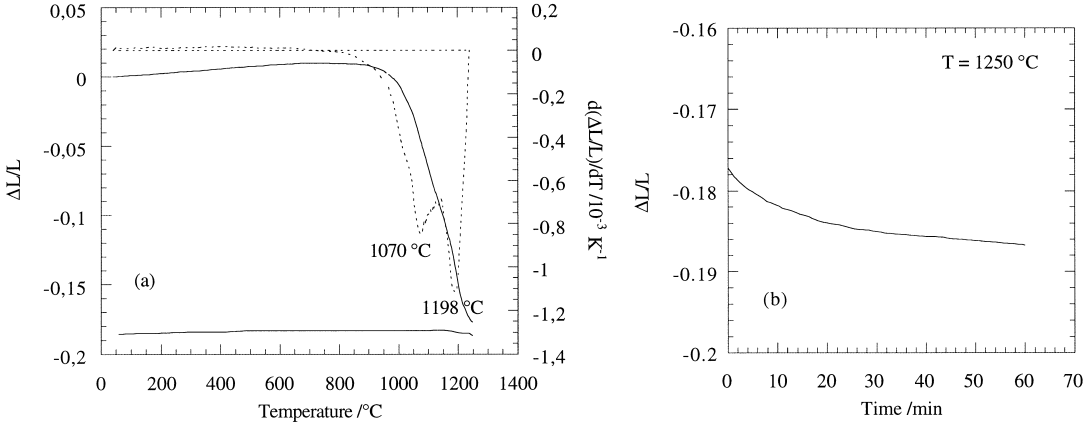


Fig. 4. Dilatometric curves for $NaNbO_3$ powder. (a) Heating and cooling stages; (b) isothermal level at 1250°C.

boundaries), corresponding to the final stage of sintering, may account for the second densification peak. According to Fig. 6, samples sintered at 1250°C for 2 h in air were highly dense but contained regions of exaggerated grain growth. Moreover, there was a large increase in the densification rate at temperatures above 1150°C (Fig. 5). The possible formation of an eutectic compound within this temperature range is another factor which might lead to both an increase of the densification rate and a reduction of the densification temperature. If one refers to the phase diagram of the $Nb_2O_5$–$Na_2O$ system,[55] one would expect an eutectic reaction at 1230°C, with $Nb_2O_5$ as a second phase. The XRD analysis confirmed that no additional crystalline phase (e.g. $Nb_2O_5$) formed during calcination (see Section 3.2). However, composition fluctuations of trace impurities can give rise locally to sufficiently concentrated zones to form a liquid phase at the boundaries. After sintering at 1250°C for 2 h in air, no traces of second phase was detected on the polished surfaces (Fig. 6). Moreover, no rounded grains, suggesting liquid-phase sintering, were evidenced. We should point out that no quenched samples (from the sintering temperatures) were examined. Hence, only a transient liquid-phase sintering might be considered.

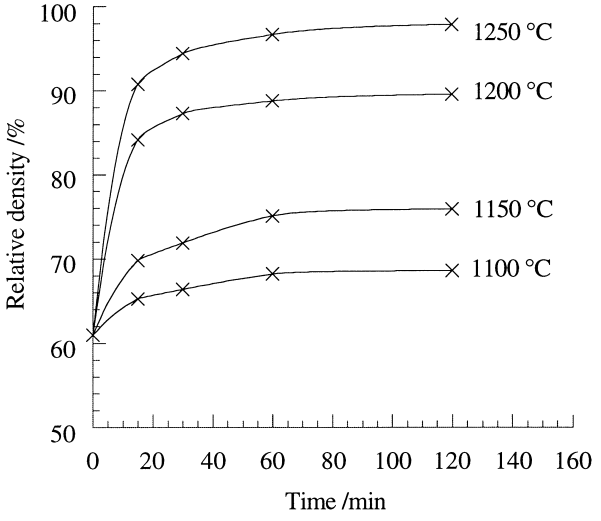


Fig. 5. Isothermal densification behaviour of $NaNbO_3$ compacts as a function of time.

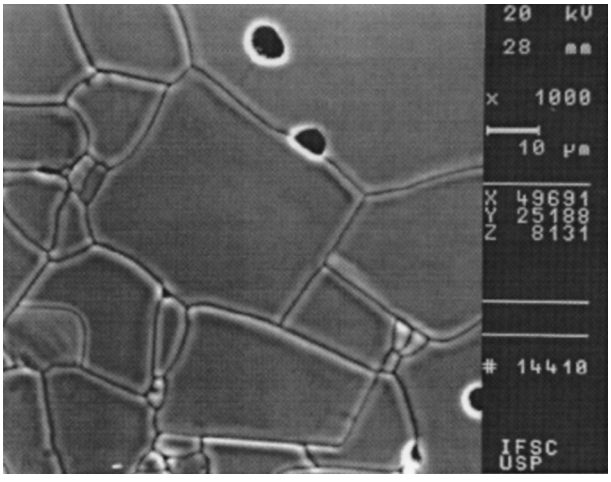


Fig. 6. SEM micrograph of a polished section of a $NaNbO_3$ compact sintered at 1250°C for 2 h in air. The relative density is 98% of the theoretical.

Fig. 5 shows the isothermal densification behaviour of calcined powders, compacted according to the chosen compaction sequence, at temperatures varying between 1100 and 1250°C for soaking times up to 2 h, in air. The green densities were of the order of 60% of the theoretical one. For all temperatures, the relative density is an increasing function of dwell time. In agreement with the dilatometric study [Fig. 4(a)], the higher the sintering temperature, the higher the density, whatever the soaking time was. Moreover, an increase in the temperature led to an increase in the densification rate. The relative density was 68% of the theoretical one after 1 h firing at 1100°C, reaching a value of 96% at 1250°C for the same duration. Further heating increased the density slightly. After 2 h at 1250°C, the relative density was 98% of the theoretical one.

### 3.6. Final microstructure

Fig. 6 shows the final microstructure of a $NaNbO_3$ compact sintered at 1250°C for 2 h in air. The relative density of the sintered sample is 98% of the theoretical density. The micrograph was taken on a surface polished with alumina powders down to 0.3 μm. The grain boundaries were revealed by thermal etching in air for 30 min at 1150°C. The microstructure consists mainly of large grains but smaller grains can also be seen. The size of large grains can reach 80 μm and that of small grains varies between 10 and 40 μm. Very few intergranular and intragranular pores can be observed, which is compatible with the final density.

## 4. Conclusion

Dense $NaNbO_3$ ceramics were prepared from powders obtained by evaporation of a solution. This evaporative method is an excellent way to prepare stoichiometric, homogeneous and fine powders, requiring neither drastic experimental conditions nor costly products. However, low pH values of the solution are needed to prevent the sodium and ammonium oxalates or niobium pentoxide from precipitating. The thermal decomposition of the precursor and the XRD study showed that the crystallization of the orthorhombic sodium niobate phase occured around 400°C. For calcination temperatures ranging between 450 and 900°C, the mean crystallite size was found to increase from 32

to 85 nm. The as-prepared powders exhibited an attractive compaction behaviour. The green density reached approximately 53% of the theoretical density for a pressure of 100 MPa, and about 60% for a pressure of 210 MPa. Two duplex shrinkage peaks were evidenced by dilatometric measurements, but high sinterability was achieved within a narrow temperature interval. The maximum shrinkage rate was found at 1200°C. Moreover, the density was at least 95% of the theoretical one after sintering at 1250°C for 2 h in air. This preparation method was also used successfully to prepare (Na,Li)$NbO_3$ and (Na,K)$NbO_3$ solid solutions. The study of the electric and dielectric properties of these electroceramics is currently underway.

## References


1. Megaw, H. D., The seven phases of sodium niobate. *Ferroelectrics*, 1974, **7**, 87–89.
2. Seidel, P., Bomas, H. and Hoffmann, W., Temperature dependence of the birefregence at the phase transition of $NaNbO_3$ P-$NaNbO_3$ N′. *Ferroelectrics*, 1978, **18**, 243–248.
3. Glazer, A. M. and Megaw, H. D., The structure of sodium niobate ($T_2$) at 600°C, and the cubic-tetragonal transition in relation to soft-phonon modes. *Phil. Mag*., 1972, **25**, 1119–1135.
4. Ahtee, M., Glazer, A. M. and Megaw, H. D., The structures of sodium niobate between 480 and 575°C, and their relevance to soft-phonon modes. *Phil. Mag*., 1972, **26**, 995–1014.
5. Nitta, T., Properties of sodium-lithium niobate solid solution ceramics with small lithium concentrations. *J. Am. Ceram. Soc*., 1968, **51**(11), 626–629.
6. Hardiman, B., Henson, R. M., Reeves, C. P. and Zeyfang, R. R., Hot pressing of sodium lithium niobate ceramics with perovskite-type structures. *Ferroelectrics*, 1976, **12**, 157–159.
7. Henson, R. M., Zeyfang, R. R. and Kiehl, K. V., Dielectric and electromechanical properties of (Li,Na)$NbO_3$ ceramics. *J. Am. Ceram. Soc*., 1977, **60**(1–2), 15–17.
8. Zeyfang, R. R., Henson, R. M. and Maier, W. J., Temperature- and time-dependent properties of polycrystalline (Li,Na)$NbO_3$ solid solutions. *J. Applied Phys*., 1977, **48**(7), 3014–3017.
9. Von der Mühll, R., Sadel, A., Ravez, J. and Hagenmuller, P., Etude des transitions ferroélectrique-paraélectrique des composés du système $NaNbO_3$-$LiNbO_3$. *Solid State Comm*., 1979, **31**, 151–156.
10. Kimura, T., Miyamoto, S. and Yamaguchi, T., Microstructure development and dielectric properties of potassium strontium niobate ceramics. *J. Am. Ceram. Soc*., 1990, **73**(1), 127–130.
11. Ding, S. and Shen, J., Microstructures and dielectric properties of pure and doped $KNbO_3$ ceramics. *J. Am. Ceram. Soc*., 1990, **73**(5), 1449–1450.
12. Wang, C. L., Zhang, P. L., Zhong, W. L. and Zhao, H. S., Dielectric and pyroelectric properties of lithium sodium niobate ceramics at low temperature. *J. Appl. Phys*., 1991, **69**(4), 2522–2524.
13. Kus, C., Ptak, W. S. and Smiga, W., Phase transitions in $Li_xNa_{1-x}$ $NbO_3$ solid solutions for $0 < x < 0.1$. *Ferroelectrics*, 1991, **124**, 249–254.
14. Dungan, R. H. and Golding, R. D., Metastable ferroelectric sodium niobate. *J. Am. Ceram. Soc*., 1964, **47**(2), 73–76.
15. Wang, C. L., Wang, Y. G., Zhang, P. L., Zhong, W. L. and Zhao, H. S., Elastic properties of sodium lithium niobate piezoelectric ceramics at low temperature. *Solid State Comm*., 1993, **85**(4), 331–333.
16. Egerton, L. and Dillon, D. M., Piezoelectric and dielectric properties of ceramics in the system potassium sodium niobate. *J. Am. Ceram. Soc*., 1959, **42**(9), 438–442.
17. Ahn, Z. S. and Schulze, W. A., Conventionally sintered ($Na_{0.5}K_{0.5}$)$NbO_3$ with barium additions. *J. Am. Ceram. Soc*., 1987, **70**(1), C18–C-21.
18. Kosec, M. and Kolar, D., On activated sintering and electrical properties of $NaKNbO_3$. *Mat. Res. Bull*., 1975, **10**, 335–340.
19. Kus, C., Dambelkane, M. J. and Brante, I. V., Production and properties of ferroelectric materials based on $NaNbO_3$ and solid solutions $Na_{1-x}Li_xNbO_3$. *Ferroelectrics*,, 1988, **81**, 281–284.
20. Todorovic, M. and Radonjic, Lj., Electrical and optical properties of ferroelectric glass-ceramics based on $LiNbO_3$ and its solid solution crystals.. In *Fourth Euro-Ceramics, vol. 5*, ed. G. Gusmano and E. Traversa. Gruppo Editoriale Faenza Editrice SpA, Faenza, 1995, pp. 253–260.
21. Johson Jr., D. W., Non conventional powder preparation techniques. *Am. Ceram. Soc. Bull*., 1981, **60**(2), 221–225.
22. Dawson, W. J., Hydrothermal synthesis of advanced ceramic powders. *Am. Ceram. Soc. Bull*., 1988, **67**(10), 1673–1678.
23. Nobre, M. A. L., Longo, E., Leite, E. R. and Varela, J. A., Synthesis and sintering of ultrafine $NaNbO_3$ powder by use of polymeric precursors. *Mat. Letters*,, 1996, **28**, 215–220.
24. Zagheto, M. A., Paiva Santos, C. O., Varela, J. A., Longo, E. and Mascarenhas, Y. P., Phase characterization of lead zirconate titanate obtained from organic solutions of citrates. *J. Am. Ceram. Soc*., 1992, **75**(8), 2088–2095.
25. Miot, C., Proust, C. and Husson, E., Dense ceramics of $BaTiO_3$ produced from powders prepared by a chemical process. *J. Eur. Ceram*., 1995, **15**, 1163–1170.
26. Lanfredi, S., Folgueras-Dominguez, S. and Martins Rodrigues, A. C., Preparation of $LiNbO_3$ powder from the thermal decomposition of a precursor salt obtained by an evaporative method. *J. Mater. Chem*., 1995, **5**(11), 1957–1961.
27. Watanabe, A., Haneda, H., Moriyoshi, Y., Shirasaki, S., Kuramoto, S. and Yamamura, H., Preparation of lead magnesium niobate by a coprecipitation method. *J. Mat. Sci*., 1992, **27**, 1245–1249.
28. Marta, L., Zaharescu, M., Haiduc, I. and Macarovici, C., Synthesis of strontium metaniobate by a coprecipitation method. *Revue Roumaine de chimie* (11–12), 957–966.
29. Cullity, B. D., *Elements of X-ray Diffraction*, 3rd edition, Addison-Wesley, New York, 1967, p. 262.
30. Muller, M. and Dehand, J., Oxalato-niobates et-tantalates de sodium. I. Obtention, conditions d'existence et caractérisation des différents complexes. *Bull. Soc. Chim Fr*., 1971, **8**, 2837–2842.
31. Marta, L., Zaharescu, M. and Macarovici, C. Gh., Thermal and structural investigation of some oxalato-niobium complexes. III. Strontium tris(oxalato)oxoniobate. *J. Therm. Anal*., 1983, **26**, 87–94.
32. Marta, L., Zaharescu, M. and Macarovici, C.Gh., Thermal and structural investigation of some oxalato-niobic complexes. I. Potassium tris(oxalato)niobate. *Revue Roumaine de Chimie*, 1979, **24**(8), 1115–1122.
33. Jorand, Y., Taha, M., Missiaen, J. M. and Montanaro, L., Compaction and sintering behaviour of sol–gel powders. *J. Eur. Ceram. Soc*., 1995, **15**, 469–477.
34. Powder Diffraction File, Card No. 33-1270. Joint Committee on Powder Diffraction Standards, Swarthmore, PA.
35. Matsumoto, R. L. K., Generation of powder compaction response diagrams. *J. Am. Ceram. Soc*., 1986, **69**(10), C-246–C-247.
36. Matsumoto, R. L. K., Analysis of powder compaction using a compaction rate diagram. *J. Am. Ceram. Soc*., 1990, **73**(2), 465–468.
37. Shi, J. L., Lin, Z. X., Qian, W. J. and Yen, T. S., Characterization of agglomerate strength of coprecipitated superfine zirconia powders. *J. Eur. Ceram. Soc*., 1994, **13**, 265–273.

38. Samdi, A., Durand, B., Daoudi, A., Chassagneux, F., Deloume, J. P., Taha, M., Paletto, J. and Fantozzi, G., Influence of formation pH and grinding of precursors on compaction and sintering behaviours of 3 mol% $Y_2O_3$–$ZrO_2$. *J. Eur. Ceram. Soc.*, 1994, **14**, 131–141.
39. Durán, P., Villegas, M., Capel, F., Recio, P. and Moure, C., Low-temperature sintering and microstructural development of nanocrystalline Y-TZP powders. *J. Eur. Ceram. Soc.*, 1996, **16**, 945–952.
40. Puyôo-Castaings, N., Duboudin, F. and Ravez, J., Elaboration of $LiNbO_3$ ceramics from sol-gel powders. *J. Mat. Res.*, 1988, **3**(3), 557–560.
41. Jeager, R. E. and Egerton, L., Hot pressing of potassium-sodium niobate. *J. Am. Ceram. Soc.*, 1963, **45**(5), 209–213.
42. Buscaglia, V., Nanni, P., Battilana, G., Aliprandi, G. and Carry, C., Reaction sintering of aluminium titanate: I. Effect of MgO addition. *J. Eur. Ceram. Soc.*, 1994, **13**, 411–417.
43. Watari, K., Yasuoka, M., Valecillos, M. C. and Kanzaki, S., Reaction process and densification process of mixed α′/β′-Sialon ceramics. *J. Eur. Ceram. Soc.*, 1995, **15**, 173–184.
44. Shi, J. L., Gao, J. H., Li, B. S. and Yen, T. S., Processing of nano-Y-TZP/$Al_2O_3$ composites II: Compaction and sintering behaviour of nano-Y-TZP/$Al_2O_3$ composite powders. *J. Eur. Ceram. Soc.*, 1995, **15**, 967–973.
45. Hidber, P., Baader, F., Graule, Th. and Gauckler, L. J., Sintering of wet-milled centrifugal cast alumina. *J. Eur. Ceram. Soc.*, 1994, **13**, 211–219.
46. Selçuk, A., Leach, C. and Rawlings, R. D., Processing, microstructure and mechanical properties of SiC platelet-reinforced 3Y-TZP composites. *J. Eur. Ceram. Soc.*, 1995, **15**, 33–43.
47. Le Calvé-Proust, C., Husson, E., Odier, P. and Coutures, J. P., Sintering ability of $BaTiO_3$ powders elaborated by citric process. *J. Eur. Ceram. Soc.*, 1993, **12**, 153–157.
48. Sato, E. and Carry, C., Effect of powder granulometry and pretreatment on sintering behavior of submicron-grained α-alumina. *J. Eur. Ceram. Soc.*, 1995, **15**, 9–16.
49. Huisman, W., Graule, T. and Gauckler, L. J., Centrifugal slip casting of zirconia (TZP). *J. Eur. Ceram. Soc.*, 1994, **13**, 33–39.
50. Rhodes, W. H. and Agglomerate, particle sizes effects on sintering of yttria-stabilized zirconia, *J. Am. Ceram. Soc.*, 1981, **64**(1), 19–22.
51. Lange, F. F., Sinterability of agglomerated powders. *J. Am. Ceram. Soc.*, 1984, **67**(2), 83–89.
52. Zheng, J. and Reed, J. S., Effects of particle packing characteristics on solid-state sintering. *J. Am. Ceram. Soc.*, 1989, **72**(5), 810–817.
53. Kang, S.-J. L., Kim, K.-H. and Yoon, D. N., Densification and shrinkage during liquid-phase sintering. *J. Am. Ceram. Soc.*, 1991, **74**(2), 425–427.
54. Hérard, C., Faivre, A. and Lemaître, J., Surface decontamination treatments of undoped $BaTiO_3$ – Part II: influence on sintering. *J. Eur. Ceram. Soc.*, 1995, **15**, 145–153.
55. Irle, E., Blachnik, R. and Gather, B., The phase diagrams of $Na_2O$ and $K_2O$ with $Nb_2O_5$ and the ternary system $Nb_2O_5$–$Na_2O$–$Yb_2O_3$. *Thermochimica Acta,*, 1991, **179**, 157–169.